Solvent Effects on the Vibrational Frequencies of the Phenolate Anion, the *para*-Cresolate Anion, and Their Radicals

William J. McDonald* and Ólöf Einarsdóttir

Department of Chemistry and Biochemistry, University of California, Santa Cruz, California 95064

Received: January 8, 2008; Revised Manuscript Received: July 11, 2008

The effects of aqueous solvation on the structure and vibrational frequencies of phenol, *para*-cresol, and their respective radicals are calculated at the B3LYP/6-31+G(d,p) level of theory using the conductor-like polarizable continuum model (C-PCM) alone and in combination with an explicit water molecule H-bonded to the phenolic oxygen. Calculated vibrational frequencies are compared to experimental frequencies obtained in aqueous buffer at high pH. For all models, the C-PCM provides the best overall agreement between theory and experiment at a modest computational effort, as demonstrated by the lowest mean absolute deviations in the computed frequencies. In addition, the C-PCM provides anion Wilson mode 7a ^{18}O isotope shifts in excellent agreement with experiment and improves agreement between the computed and observed radical Wilson mode 7a ^{2}H isotope shift. On the basis of a quantitative comparison of the anion and radical normal modes by vibrational projection analysis and total energy decomposition, an alternative criterion for distinguishing the anion and radical Wilson modes 7a and 19a using the relative phasing of the carbon−oxygen and carbon−carbon bond stretches is presented.

Introduction

Redox-active tyrosine residues have been identified in a number of enzymes such as photosystem II[1,2] (PSII), cytochrome *c* oxidase[3,4] (C*c*O), ribonucleotide reductase,[5] and prostaglandin H synthase.[6] Tyrosine residues are found with and without post-translational modification, which include, for example, the cysteine-tyrosine moiety of galactose oxidase[7] and the histidine-tyrosine biring structure observed in cytochrome *c* oxidase.[4] These covalent modifications serve to fine-tune the chemical and physical properties of tyrosine, such as the midpoint potential[2,8] or the phenolic pK_a,[9] to suit a specific enzymatic function.

A variety of spectroscopic methods has been fruitfully applied to such enzyme systems. Infrared spectroscopy, particularly difference−absorbance methods, have been used to understand nuclear motions involved in enzymatic turnover.[10] In addition, time-resolved optical absorbance and resonance Raman measurements have elucidated intermediates and transient chemical species, for example, in cytochrome *c* oxidase.[11−16] Electron paramagnetic resonance (EPR) spectroscopy has also been used to understand the nature of electron transfer and the generation of radicals in enzymes.[17]

While significant progress has been made, these direct measurements are limited by the complex spectra and the large number of variables and degrees of freedom. For this reason, much work has focused on model compounds such as free tyrosine residues[18,19] or truncated tyrosine models like phenol[20−22] and *para*-cresol (4-methylphenol).[23] These simple models capture much of the relevant chemistry; for example, it is known[24] that photolytic oxidation of tyrosine generates a π-radical. EPR measurements[25,26] have revealed that the majority of spin density is localized onto the phenol ring. This indicates that the most pronounced features of the tyrosyl EPR spectrum arise from phenol and its properties. It is therefore expected that a detailed understanding of the phenol and *para*-cresol model systems will provide insight into the general properties of tyrosine and tyrosyl radicals while drawing attention to the differences and nuances of residues in particular enzymes.

Computational studies[14,19,27−29] on tyrosine and model compounds have made significant contributions complementary to experimental work. In a recent report, Barry and co-workers[14] used several different model structures to predict the vibrational frequencies of the normal modes of tyrosine. The primary criterion for assessing the success of their model structures was the ability of the models to predict the intense 1266 cm^{-1} frequency for tyrosinate (Wilson mode 7a), attributed primarily to the phenol−oxygen bond stretching. It was found that the gas-phase oxygen-protonated tyrosine structure best reproduced the Wilson mode 7a frequency.

In the present work, the effects of solvation on the structure and vibrational spectra of phenol and 4-methylphenol (*para*-cresol), and their respective radicals, are explored using hybrid density functional theory. The two major contributions to solvation are electrostatic interactions and H-bonded interactions. In order to explore the full range of hydrogen−oxygen bond strengths, gas-phase phenolate and *para*-cresolate anions are compared to gas-phase H-bonded phenolate−water and *para*-cresolate−water complexes and to gas-phase phenol and *para*-cresol. To separate the electrostatic and H-bonded interactions, the conductor-like polarizable continuum model (C-PCM) is used alone and in combination with the phenolate−water and *para*-cresolate−water H-bonded complexes. The calculated vibrational frequencies and isotope shifts are compared to aqueous spectra of phenol, *para*-cresol, tyrosine, and their respective radicals. While the closed-shell (i.e., anionic or neutral) Wilson mode 7a frequency is correctly predicted by the gas-phase O-protonated structures, it is overestimated by the other solvation models. It is found that the simple C-PCM water-solvated models provide the best overall agreement between theory and experiment for both the closed-shell and

* Author to whom correspondence should be addressed. E-mail: mcdonald@chemistry.ucsc.edu. Telephone: (831) 459-3061. Fax: (831) 459-2935.

10.1021/jp800169w CCC: $40.75
Published on Web 10/22/2008

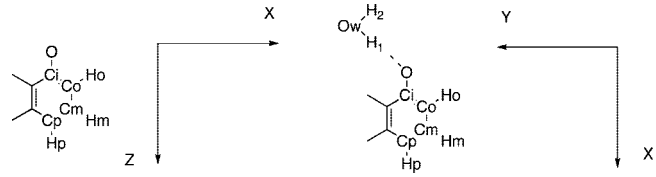

Figure 1. Atom label definitions for phenol.

radical molecules at a modest computational effort. On the basis of a quantitative comparison of the anion and radical normal modes by vibrational projection analysis and total energy decomposition, an alternative criterion for distinguishing the anion and radical Wilson modes 7a and 19a using the relative phasing of the carbon−oxygen and carbon−carbon bond stretches is presented.

Computational Method

All calculations were performed using the GAMESS[30] ab initio software suite. The B3LYP hybrid density functional was used in combination with the 6-31+G(d,p) basis[31] restricted to spherical harmonics. The B3LYP functional includes Becke's 1988 (B88)[32] gradient correction to Slater's local exchange functional,[33] Hartree−Fock (or exact) exchange, and the correlation functionals of Lee−Yang−Parr (LYP)[34] and Vosko−Wilk−Nusair (VWN5).[35] Integration over XC functionals was performed using the default grid consisting of 96 radial and 12*24 angular points per atom.

The phenolate anion and neutral radical were defined in C_{2v} symmetry, with the Cartesian *Z*-axis as the principle rotation axis and the phenol ring lying in the *XZ*-plane (see Figure 1). The H-bonded phenol−water complexes (anion and neutral radical) as well as the gas-phase phenol structure were defined in C_s symmetry, with all atoms in the *XY*-plane. *para*-Cresol and the H-bonded complexes (anion and neutral radical) were not symmetry constrained because the two possible C_s structures are transition states with respect to CH_3 rotation.

Full geometry optimizations were carried out using the "natural internal coordinates" of Pulay et al.[36] Structures are considered a stationary point when the largest Cartesian component of the nuclear energy gradient vector is less than 50 microHartree per bohr and the root-mean-square gradient is less than one-third of the largest component. At the stationary point, Hessian calculations were carried out by finite differencing of analytical nuclear gradients. Symmetry unique atoms were displaced in both positive and negative directions along each Cartesian coordinate.

Results and Discussion

Phenolate. Selected structural parameters for phenol solvation models appear in Table 1, and the atom label definitions are shown in Figure 1. The complete set of parameters is provided in Table S1 of the Supporting Information. It is clear from Table 1 that the solvation models provide small but significant changes to the anion structure. However, for all of the ionic structures, the OC_i bond length contains significant double-bond character, in agreement with the findings of Barry and co-workers,[14] and only with the gas-phase protonated structure does the bond length approach that of a prototypical O−C single bond. This is confirmed by the calculated bond orders,[37] which are 1.83, 1.45, 1.74, 1.47, and 0.94 for the gas-phase anion, C-PCM water-solvated anion (C-PCM anion), gas-phase phenolate−H_2O complex (gas-phase complex), C-PCM water-solvated phenolate−H_2O complex (C-PCM complex), and gas-phase phenol, respectively. The ionic structures also predict long C_oC_i bonds and narrow $C_o'C_iC_o$ angles, suggesting significant contributions from quinoidal resonance structures. The gas-phase O-protonated structure, however, is essentially a benzene ring with a single-bonded hydroxyl group. It will be shown (vide infra) that the quinoidal resonance structures must be included for an accurate description of the solution structure and the complete set of vibrational frequencies of aqueous phenol at high pH.

TABLE 1: B3LYP/6-31+G(d,p) Calculated Bond Lengths (Å) and Angles (°) for Phenol

	gas-phase anion	C-PCM[a] anion	gas-phase complex[b]	C-PCM[c] complex	gas-phase phenol
$R(OH_1)$			1.634	1.605	0.966
$R(OC_i)$	1.276	1.301	1.291	1.311	1.373
$R(C_oC_i)$	1.450	1.436	1.438	1.429	1.400
$R(C_mC_o)$	1.392	1.396	1.394	1.397	1.397
$R(C_pC_m)$	1.408	1.405	1.406	1.404	1.399
$A(OC_iC_o)$	123.0	122.4	122.4	122.0	122.4, 117.5
$A(C_o'C_iC_o)$	114.0	115.2	115.1	115.1	120.2
$A(C_iC_oC_m)$	122.5	122.1	122.0	121.7	119.6
$A(C_oC_mC_p)$	121.7	121.3	121.5	121.1	120.7
$A(C_m'C_pC_m)$	117.5	118.1	117.9	118.4	119.2

[a] C-PCM water-solvated phenolate anion. [b] Gas-phase phenolate−H_2O complex. [c] C-PCM water-solvated phenolate−H_2O complex.

TABLE 2: Observed and Calculated Fundamental Frequencies (in cm^{-1}) for Phenol

Wilson mode	observed	gas-phase anion	C-PCM anion	gas-phase complex	C-PCM complex	gas-phase phenol
8a	1585[a]	1624	1611	1628	1622	1644
8b	1569[b]	1541	1562	1575	1589	1635
19a	1534[b]	1542	1500	1535	1510	1525
19b	1445[a]	1473	1466	1487	1483	1492
7a	1264[a]	1399	1352	1390	1337	1281
14	1324[b]	1335	1338	1355	1353	1356
9a	1165[c]	1169	1171	1167	1167	1200
18a	1020[a]	1021	1026	1033	1039	1038
12	992[a]	971	975	992	994	1001
1	820[a]	820	829	839	842	822

[a] Raman, 514.5 nm excitation, pH 12.[18] [b] Resonance Raman, 245 nm excitation, 0.1 M NaOH.[21] [c] This mode appears at ~1165 cm^{-1} in both of the resonance spectra of the references in footnotes a and b, while it was observed at 1153 cm^{-1} in the off-resonance spectrum of the reference in footnote a.

Experimental and calculated fundamental frequencies for phenolate are listed in Table 2. The complete set of calculated frequencies is given in Table S2 of the Supporting Information. The overall agreement between theory and experiment is satisfactory. Wilson mode 18a, which is largely CH bending, mode 12, the symmetric trigonal ring deformation, and mode 1, the symmetric ring-breathing, are in good agreement for all models. For the gas-phase anion, many of the calculated frequencies are overestimated; however, the errors are not systematic. The largest error occurs with Wilson mode 7a, which is dominated by OC_i stretching. This is not surprising given

TABLE 3: Observed and Calculated Isotope Shifts (in cm^{-1})

A. ^{18}O Shifts for Phenol

ν	experiment[a]	gp anion	C-PCM anion	gp complex	C-PCM complex	gp phenol
19a	1534	1542	1500	1535	1510	1525
$\Delta\nu$		−13	−4	−8	−2	−1
7a	1264	1399	1352	1390	1337	1281
$\Delta\nu$	−18	−13	−19	−16	−19	−11

B. ^{13}C Shifts for Phenolate

ν	experiment[d]	gp anion	C-PCM	gp complex	C-PCM anion	gp phenol
8a	1585	1624	1611	1628	1622	1644
$\Delta\nu(^{13}C_6)$[b]	−51	−55	−56	−56	−56	−57
$\Delta\nu(^{13}C_1)$[c]		−10	−3	−7	−3	−7
8b	1569	1541	1562	1575	1589	1635
$\Delta\nu(^{13}C_6)$	−44	−51	−53	−53	−54	−56
$\Delta\nu(^{13}C_1)$		−5	−7	−6	−7	−15
19a	1534	1542	1500	1535	1510	1525
$\Delta\nu(^{13}C_6)$	−47	−40	−35	−39	−35	−35
$\Delta\nu(^{13}C_1)$		−23	−14	−20	−12	−8
19b	1447	1473	1466	1487	1483	1492
$\Delta\nu(^{13}C_6)$	−31	−40	−37	−39	−36	−33
$\Delta\nu(^{13}C_1)$		−2	−3	−4	−5	−7
14	1324	1335	1338	1355	1353	1356
$\Delta\nu(^{13}C_6)$	−21	−24	−24	−26	−25	−15
$\Delta\nu(^{13}C_1)$		−1	0	−1	0	−6
7a	1264	1399	1352	1390	1337	1281
$\Delta\nu(^{13}C_6)$	−36	−26	−29	−28	−31	−32
$\Delta\nu(^{13}C_1)$		−7	−21	−13	−24	−25
9a	1165	1169	1171	1167	1167	1200
$\Delta\nu(^{13}C_6)$	−5	−6	−6	−6	−6	−7
$\Delta\nu(^{13}C_1)$		0	0	0	0	0

C. ^{2}H Shifts for Phenol

ν	experiment	gp anion	C-PCM anion	gp complex	C-PCM complex	gp phenol
8a	1592[g]	1624	1611	1628	1622	1644
$\Delta\nu(^2H_5)$[e]	−39[g]	−30	−37	−33	−36	−30
$\Delta\nu(^2H_2)$[f]		−14	−11	−13	−11	−23
8b	1564[g]	1541	1562	1575	1589	1635
$\Delta\nu(^2H_5)$	−34[g]	−39	−40	−40	−40	−33
$\Delta\nu(^2H_2)$		−11	−12	−11	−11	−4
19a	1534[h]	1542	1500	1535	1510	1525
$\Delta\nu(^2H_5)$	−90[g], −131[h]	−36	−70	−49	−83	−105
$\Delta\nu(^2H_2)$		−13	−39	−25	−45	−43
19b	1483[g]	1473	1466	1487	1483	1492
$\Delta\nu(^2H_5)$	−100[g], −186[h]	−72	−86	−80	−93	−106
$\Delta\nu(^2H_2)$		−15	−15	−15	−15	−24
14	1274[g], 1324[h]	1335	1338	1355	1353	1356
$\Delta\nu(^2H_5)$	−73[g]	−95	−74	−310	−304	−11
$\Delta\nu(^2H_2)$		−21	−25	−18	−23	−1
7a	1290[g], 1264[h]	1399	1352	1390	1337	1281
$\Delta\nu(^2H_5)$	−71[g], −58[h]	−137	−98	−116	−79	−70
$\Delta\nu(^2H_2)$		−42	−19	−33	−14	−15
9a	1168[h]	1169	1171	1167	1167	1200
$\Delta\nu(^2H_5)$	n.o.	−336	−336	−331	−330	−346
$\Delta\nu(^2H_2)$		−87	−86	−76	−73	−101

[a] FT-IR phenolate, pH 12.[23] [b] Ring atoms substituted with ^{13}C. [c] C_i (see Figure 1) substituted with ^{13}C. [d] UV−resonance Raman, 245 nm excitation, 0.1 M NaOH.[21] [e] H atoms isotopically substituted with ^{2}H. [f] H_o and H_o' (see Figure 1) isotopically substituted with ^{2}H. [g] FT-IR, pH 12.[38] [h] UV−resonance Raman, 245 nm excitation, 0.1 M NaOH;[21] gp = gas-phase.

the short bond length and the large amount of double-bond character predicted.

The calculated C-PCM water-solvated anion frequencies are moderately improved over those calculated for the gas-phase anion. The largest shift of 47 cm^{-1} occurs for Wilson mode 7a. While this frequency is still in error by 6.2%, the magnitude and direction of the shift relative to the gas-phase anion and the insignificant 9 cm^{-1} downshift predicted by the gas-phase H_2O−phenolate complex support the conclusion that electrostatic interactions between solvent and solute are most important for accurately describing the solution structure and vibrational frequencies of the phenolate anion.

The most sophisticated solvation model is the C-PCM water-solvated phenolate−H_2O complex (C-PCM complex). This model includes both the specific water−phenolate intermolecular interactions as well as the anion−bulk solvent electrostatic

interactions. This model provides the largest shift in Wilson mode 7a compared to the gas-phase anion, and agreement with experiment, while not exemplary, is satisfactory (5.8% error). It is interesting to note that the combination of both electrostatic and H-bonded interactions in the C-PCM water-solvated complex shifts this mode more than the sum of the individual solvation model contributions. The remaining modes, as would be expected, provide results intermediary to the C-PCM anion and gas-phase phenolate−H_2O complex.

The gas-phase phenol structure provides the best agreement with experiment for Wilson mode 7a, in accord with the predictions of Barry and co-workers.[14] The predicted frequency of 1281 cm^{-1} is in error by only 1.3%. However, this structure overestimates many frequencies, including for example, 9a, which is correctly predicted by all of the anionic models. In fact, while the gas-phase protonated phenol model correctly predicts the 7a frequency, it has the largest mean absolute error of 29.7 cm^{-1} (2.22%) compared to 27.0 cm^{-1} (1.86%) for the gas-phase anion, 22.2 cm^{-1} (1.59%) for the C-PCM water-solvated anion, 28.1 cm^{-1} (2.00%) for the gas-phase phenolate−H_2O complex, and 26.4 cm^{-1} (1.87%) for the C-PCM water-solvated complex. It seems that while the very strong H−O interaction correctly predicts the energy of mode 7a, it leads to errors in most other frequencies, notably the ring vibrations.

Observed and calculated ^{18}O, ^{13}C, and ^{2}H isotope shifts appear in Table 3A−C. It is clear from Table 3A that all gas-phase models underestimate the 7a ^{18}O shift, while the C-PCM solvated anion and H-bonded complex correctly predict this isotope shift. It should also be noted that the gas-phase anion mode 19a ^{18}O shift is equal to the 7a shift, indicating a significant C_iO stretching contribution to mode 19a. The remaining 19a ^{18}O shifts are systematically reduced with an improved solvation model, indicating a reduced C_iO stretching contribution to this vibration.

Observed and calculated ^{13}C shifts appear in Table 3B. The overall agreement between theory and experiment is satisfactory, although the gas-phase phenol structure underestimates and all of the anionic structures overestimate the Wilson mode 14 $^{13}C_6$ shift. While there is little experimental data on the $C_i-^{13}C_1$ isotope shift for aqueous phenolate, the magnitude of these shifts, especially the 7a and 19a shifts, may be estimated from the FT-IR spectrum of aqueous tyrosinate. Barry and co-workers[14] observed an isotope shift of −24 cm^{-1} for the tyrosinate $C_i-^{13}C_1$ ($^{13}C(4')$ in ref 14) mode 7a and a shift of −9 cm^{-1} for the $C_i-^{13}C_1$ mode 19a. It may be concluded that a larger $C_i-^{13}C_1$ isotope shift occurs with mode 7a and a smaller shift with 19a. In Table 3B, the gas-phase anion and gas-phase H-bonded complex predict a larger $C_i-^{13}C_1$ isotope shift for 19a and a smaller shift for 7a, while the C-PCM solvated structures (C-PCM anion and phenolate−H_2O complex) and gas-phase phenol correctly predict a larger isotope shift for 7a and a smaller shift for mode 19a. This suggests that for the gas-phase anionic structures, there is a significant C_iO stretching contribution to mode 19a. Furthermore, the observation that the C-PCM solvated structures correctly predict the relative magnitude of these two isotope shifts suggests that electrostatic solvation models provide a simple means of capturing many of the solvent−solute interactions.

The ^{2}H isotope shifts appear in Table 3C. The gas-phase anion, gas-phase phenolate−H_2O complex, and phenol underestimate mode 8a $^{2}H_5$ shifts, while the C-PCM water-solvated models (anion and phenolate−H_2O complex) provide better results. The mode 8b $^{2}H_5$ gas-phase phenol shift is in good agreement with experiment, while all anionic models overestimate this shift. The very large shifts predicted for mode 9a help explain why this shift is not observed experimentally. The large $^{2}H_5$ shift for 19b of −186 cm^{-1} in the UV−resonance Raman spectrum of Spiro and co-workers[15] is questionable as this shift is −100 cm^{-1} in the phenolate FT-IR spectrum[38] and −59 cm^{-1} for *para*-cresol in a nonpolar solvent.[39] In addition, there is a weak, broad peak at 1350 cm^{-1} in the phenolate UV−resonance Raman spectrum of Spiro and co-workers,[15] which is in better agreement with the phenolate FTIR[33] and *para*-cresol isotope shifts. The 19a $^{2}H_5$ isotope shift is −131 cm^{-1} in the UV−resonance Raman spectrum of the aqueous phenolate anion,[15] while the phenolate difference FT-IR spectrum of Berthomieu and Boussac[33] suggests a deuterium shift of −90 cm^{-1}. The aqueous FT-IR spectrum of tyrosinate[14] agrees with the latter assignment, with this shift reported as −80 cm^{-1}. Spiro and co-workers[15] report a mode 7a $^{2}H_5$ isotope shift of −58 cm^{-1}, while in the difference FT-IR spectrum of aqueous phenolate,[33] this shift is reported to be −71 cm^{-1}, and Barry and co-workers[14] report a −30 cm^{-1} shift for tyrosinate. While there is little agreement as to the magnitude of the shifts, the larger $^{2}H_5$ shift has been assigned to 19a and the smaller to 7a. From Table 3C, only the gas-phase phenol structure predicts a large $^{2}H_5$ shift for 19a and a significantly smaller shift for 7a.

On the basis of the above analysis, it may appear that the deuterium shifts are missassigned; however, vibrational projection analysis[40] supports the above assignment. For the gas-phase anion, the projection coefficients of the deuterated modes 19a and 7a onto the natural abundance modes 19a and 7a are 0.913 (83%) and 0.897 (80%), respectively. The corresponding coefficients for the C-PCM anion are 0.900 (81%) and 0.956 (91%). These large, near-unit coefficients indicate that there is one-to-one mapping of the deuterium modes onto the natural abundance normal coordinates. This is not the case for the remaining three phenol structures; for the gas-phase phenolate−H_2O complex, the C-PCM water-solvated complex, and the gas-phase phenol, the projection coefficients of the deuterated mode 19a onto the natural abundance mode 19a are 0.693 (48%), 0.590 (35%), and 0.619 (38%), respectively, and the 7a coefficients are 0.479 (23%), 0.496 (25%), and 0.490 (24%), respectively. In addition, the coefficients for the projection of the deuterated mode 19a onto the natural abundance mode 7a are 0.570 (32%), −0.704 (50%), and 0.542 (29%) for the gas-phase phenolate−H_2O complex, the C-PCM water-solvated complex, and the gas-phase phenol, respectively. This suggests that for structures that include H−O bonds, both of the natural abundance 19a and 7a modes contribute to the deuterated mode 19a, and there is no unique Wilson mode 19a for these isotope-substituted structures. Furthermore, both of the C-PCM water-solvated structures predict nearly equal $^{2}H_5$ shifts of −98 and −70 cm^{-1} (C-PCM water solvated anion) and −79 and −83 cm^{-1} (C-PCM water-solvated phenolate−H_2O complex) for modes 7a and 19a, respectively, while the gas-phase anion and gas-phase H-bonded complex predict a large shift for 7a (−137 and −116 cm^{-1}) and a small shift for 19a (−36 and −49 cm^{-1}). For the latter models, the deuterated Wilson mode 7a contains 5.6 and 3.1% natural abundance C−H bending mode 9a, respectively. The C-PCM structures and gas-phase phenol, by contrast, contain negligible contributions from this mode. It may be the admixture of the C−H bending mode 9a into the deuterated mode 7a that leads to the incorrectly calculated isotope shifts for the gas-phase anion and H-bonded complex.

TABLE 4: Calculated Bond Lengths (Å) and Angles (°) for Phenolate−H_2O Complexes

	gas-phase phenolate−H_2O complex			C-PCM phenolate−H_2O complex		
	B3LYP	X3LYP	PBE0	B3LYP	X3LYP	PBE0
$R(OO_w)$	2.643	2.635	2.619	2.617	2.609	2.593
$R(OH_1)$	1.634	1.626	1.613	1.605	1.597	1.583
$R(OC_i)$	1.291	1.290	1.284	1.311	1.310	1.302
$R(C_oC_i)$	1.438	1.437	1.433	1.429	1.428	1.425
$R(C_mC_o)$	1.394	1.392	1.389	1.397	1.396	1.392
$R(C_pC_m)$	1.406	1.405	1.401	1.404	1.403	1.400
$A(OC_iC_o)$	122.4	122.4	122.5	122.0	121.9	122.0
$A(C_o'C_iC_o)$	115.1	115.2	115.1	116.1	116.1	116.0
$A(C_iC_oC_m)$	122.0	122.0	122.1	121.7	121.7	121.7
$A(C_oC_mC_p)$	121.5	121.4	121.5	121.1	121.1	121.1
$A(C_m'C_pC_m)$	117.9	117.9	117.8	118.4	118.4	118.3

TABLE 5: Observed and Calculated Fundamental Frequencies (cm^{-1}) for Phenolate−H_2O Complexes

		gas-phase phenolate−H_2O complex			C-PCM phenolate−H_2O complex		
Wilson mode	observed	B3LYP	X3LYP	PBE0	B3LYP	X3LYP	PBE0
8a	1585[a]	1628	1634	1662	1622	1628	1653
8b	1569[b]	1575	1581	1605	1589	1595	1618
19a	1534[b]	1535	1540	1565	1510	1514	1530
19b	1445[a]	1487	1491	1504	1483	1487	1498
7a	1265[a]	1390	1395	1408	1337	1342	1368
14	1318[a]	1355	1358	1373	1353	1356	1372
9a	1165[b]	1167	1169	1168	1167	1169	1167
18a	1020[a]	1033	1036	1047	1039	1042	1051
12	992[a]	992	994	997	994	997	1000
1	820[a]	839	842	851	842	845	853

[a] Raman, 514.5 nm excitation, pH 12.[18] [b] Resonance Raman, 245 nm excitation, 0.1 M NaOH.[21]

It has been shown[41,42] that the B3LYP functional underbinds weakly interacting systems such as H-bonded complexes. To explore the functional dependence of the calculated structures and vibrational frequencies, calculations were repeated for the phenolate−H_2O complexes using the X3LYP[36] and PBE0[43] hybrid density functionals and the same 6-31+G(d,p) basis set. Selected structural parameters appear in Table 4. It is clear that the water−phenolate $O-O_w$ separation and the phenolate $O-H_1$ bond lengths are smaller using the X3LYP and PBE0 functionals compared to those using the B3LYP functional, suggesting tighter binding. However, the X3LYP OC_i bond length is unchanged from the B3LYP value, and the PBE0 functional predicts a shorter OC_i bond length. The remaining phenolate structural parameters are unchanged.

Calculated vibrational frequencies for the gas-phase and C-PCM water-solvated phenolate−H_2O complexes using the B3LYP, X3LYP, and PBE0 functionals appear in Table 5. The X3LYP frequencies are not significantly different from the B3LYP results, while the PBE0 functional consistently overestimates vibrational frequencies.

***para*-Cresolate.** Selected structural parameters for *para*-cresol appear in Table 6, and the atom label definitions are shown in Figure 2. The complete set of structural parameters appears in Table S3 of the Supporting Information. It is clear from Table 6 that *para*-cresol has near-C_s symmetry about the benzyl plane, but the H_a methyl hydrogen is rotated ~8° out of the benzyl plane. In the calculated *para*-cresol and phenol structures, equivalent bond lengths are changed by less than 1 pm and angles by less than 1°, and it may be concluded that the *para*-cresolate anion has significant contributions from quinoidal resonance structures. These structural similarities also suggest that the ring vibrations should be similar in energy. It should be noted that solvation does not significantly alter the structure of the methyl substituent, suggesting that vibrations involving the methyl moiety should not change too much across the solvation model.

TABLE 6: B3LYP/6-31+G(d,p) Calculated Bond Lengths (Å) and Angles (°) for *para*-Cresol

	gas-phase anion	C-PCM[a] anion	gas-phase complex[b]	C-PCM complex[c]	gas-phase cresol
$R(OH_1)$			1.637	1.589	0.966
$R(OC_i)$	1.277	1.305	1.291	1.317	1.374
$R(C_oC_i)$	1.448	1.433	1.437	1.426	1.398
$R(C_mC_o)$	1.393	1.397	1.394	1.397	1.397
$R(C_pC_m)$	1.409	1.407	1.407	1.406	1.403
$R(C_{Me}C_p)$	1.514	1.515	1.514	1.515	1.513
$A(OC_iC_o)$	123.3	122.7	122.8	122.3	122.5,117.9
$A(C_o'C_iC_o)$	113.4	114.6	114.5	115.4	119.6
$A(C_iC_oC_m)$	122.7	122.3	122.2	121.9	119.8
$A(C_oC_mC_p)$	122.6	122.3	122.4	122.2	121.7
$A(C_m'C_pC_m)$	117.5	118.1	117.9	118.4	119.2
$A(C_{Me}C_pC_m)$	122.0	121.8	121.9	121.8	121.3
$\tau(H_aC_{Me}C_pC_m)$	7.6	7.4	8.3	7.7	7.6

[a] C-PCM water-solvated *para*-cresolate anion. [b] Gas-phase *para*-cresolate−H_2O complex. [c] C-PCM water-solvated *para*-cresolate−H_2O complex.

Observed and calculated fundamental frequencies for *para*-cresol are presented in Table 7. The complete set of calculated frequencies appears in Table S4 of the Supporting Information. The mean absolute errors for *para*-cresol and phenol are similar in magnitude, and the type of error (i.e., over- or underestimation) is consistent for each mode and solvation model. For *para*-cresol, the C-PCM water-solvated complex and C-PCM anion perform equally well, with the smallest mean absolute errors of 23.2 (1.81%) and 23.9 cm^{-1} (1.87%), respectively. The gas-phase anion has the largest mean absolute error of 39.6 cm^{-1} (3.1%), and the gas-phase complex and O-protonated structures are intermediary, with mean absolute errors equal to 34.6 (2.7%)

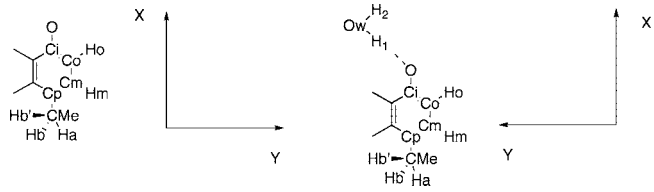

Figure 2. Atom label definitions for *para*-cresol.

TABLE 7: Observed and Calculated Fundamental Frequencies (in cm^{-1}) for *para*-Cresol

Wilson mode	observed	gas-phase anion	C-PCM anion	gas-phase complex	C-PCM complex	gas-phase cresol
8a	1606[a]	1640	1636	1643	1638	1660
8b	1555[a]	1537	1556	1556	1567	1634
19a	1501[a]	1560	1519	1548	1521	1551
19b	1425[b]	1449	1437	1450	1437	1454
7a′	1267[a]	1411	1348	1395	1321	1284
7a	1217[b]	1227	1230	1229	1228	1235
9a	1173[a]	1193	1195	1196	1198	1214
14	1291[b]	1329	1328	1333	1331	1338
18a	1014[b]	975	983	988	993	1018
1	842[b]	832	843	846	848	850

[a] Difference FTIR, pH 12.[23] [b] FTIR, 50 mM cresol in carbon disulfide and dichloroethene.[39]

and 34.8 cm^{-1} (2.5%), respectively. Again, the simple electrostatic model of solvation provides the most accurate results; however, for *para*-cresol, the gas-phase O-protonated structure is more accurate than that of the gas-phase anion.

In the aqueous difference FTIR spectrum of *para*-cresol, Berthomieu et al.[17] observed two intense modes at 1501 and 1267 cm^{-1} that were assigned as 19a and 7a′, respectively. Low-intensity modes observed at 1606 and 1173 cm^{-1} were assigned as 8a and 9a, respectively. In the aqueous FTIR absorbance spectrum of tyrosinate,[14,44] intense modes were observed at 1500 and 1266 cm^{-1} and medium intensity modes at 1600 and ~1415 cm^{-1}. Barry and co-workers[14] report a low-intensity tyrosinate mode at 1173 cm^{-1} that is not reported by Hellwig et al.[36] These observed tyrosinate frequencies are in good agreement with those observed for *para*-cresol and the present calculations.

Observed and calculated *para*-cresol isotope shifts appear in Table 8A−C. The ^{18}O isotope shifts appear in Table 8A. A similar pattern is found for the *para*-cresol ^{18}O isotope shifts as was observed for phenolate, and similar conclusions may be reached. The gas-phase anion predicts equal shifts for modes 7a and 19a, suggesting significant OC_i stretching in these two modes; the 19a ^{18}O shifts decrease with an improved solvation model, resulting in better agreement with experiment; and the gas-phase anion and *para*-cresol underestimate the 7a shift. As was observed with phenolate, the C-PCM solvated models provide ^{18}O shifts in good agreement with experiment.

Calculated ^{13}C shifts appear in Table 8B. Experimental ^{13}C isotope shift data are sparse for the aqueous *para*-cresolate anion; however, the relative magnitude of the shifts may be obtained from aqueous tyrosinate. For Wilson mode 8a, Barry and co-workers[14] report the $^{13}C_6$ isotope shift as −53 cm^{-1} and the $C_i-^{13}C_1$ shift ($^{13}C(4')$ in ref 14) as −3 cm^{-1}, in good agreement with our calculations. The observed[14] mode 7a $C_i-^{13}C_1$ ($^{13}C(4')$ in ref 14) tyrosinate isotope shift is −24 cm^{-1}, and the $^{13}C_6$ shift is −28 cm^{-1}. From Table 8B, the mode 7a $^{13}C_6$ isotope shifts are in reasonable agreement with the above tyrosinate shifts, while the gas-phase anionic structures predict smaller $C_i-^{13}C_1$ isotope shifts. The C-PCM water-solvated models and gas-phase *para*-cresol predict larger 7a $C_i-^{13}C_1$ shifts, in better agreement with expectations. The experimental tyrosinate[14] mode 19a $C_i-^{13}C_1$ shift is −9 cm^{-1}, and the $^{13}C_6$ shift is −36 cm^{-1}. For Wilson mode 19a, the calculated $^{13}C_6$ isotope shifts are reasonable; however, the gas-phase anion and gas-phase *para*-cresolate−H_2O complex overestimate the $C_i-^{13}C_1$ isotope shifts. The C-PCM solvated models and gas-phase *para*-cresol predict 19a $C_i-^{13}C_1$ isotope shifts in good agreement with expectations. As was observed with phenolate, the gas-phase anionic structures predict large C_iO stretching contributions to mode 19a, and inclusion of an electrostatic solvation model reduces this contribution, showing improved agreement with experiment.

Observed and calculated ^2H isotope shifts for *para*-cresolate appear in Table 8C. Mode 8a ^2H shifts are in excellent agreement with experimental[34] shifts obtained in nonpolar solvent, indicating that this isotope shift is insensitive to solvent effects. The very large shifts predicted for Wilson mode 9a show reasonable agreement with experimental data obtained in nonpolar solvent. All calculated isotope shifts are 10−15% too large and independent of the solvent model. The ^2H shifts of modes 7a and 19a show a similar pattern as observed for phenol. The gas-phase anionic models predict a larger $^2H_4$ shift for 7a than for 19a, while the gas-phase *para*-cresol correctly predicts a larger shift for 19a and a smaller shift for mode 7a. Unlike for phenolate, however, both C-PCM solvated *para*-cresolate structures correctly predict a larger $^2H_4$ shift for 19a and a smaller shift for 7a.

While the mean absolute errors in the calculated frequencies are larger for *para*-cresol than those for phenol, the remaining spectral data for *para*-cresol are in better agreement with observations. In particular, the *para*-cresol isotope shifts are in much better agreement with experiment. In addition, the calculated *para*-cresolate frequencies and isotope shifts compare well to those of aqueous tyrosinate, suggesting that *para*-cresol is a satisfactory model for the tyrosinate anion.

Phenoxyl Radical. Selected structural parameters for the phenoxyl radical appear in Table 9. The atom labels are those defined in Figure 1. The complete set of structural parameters appears in Table S5 of the Supporting Information. The gas-phase radical structure of the present investigation agrees well with the UB3LYP/cc-pVTZ calculations of Radziszewski and co-workers,[15] with mean deviations of 0.7 pm (7×10^{-3} Å) in bond lengths and 0.03° in angles, indicating that the gas-phase structure is nearly converged with respect to the basis set at the UB3LYP/6-31+G(d,p) level. As would be expected, solvation

TABLE 8: Observed and Calculated Isotope Shifts (in cm^{-1})

A. ^{18}O Shifts for *para*-Cresol

ν	experiment	gp anion	C-PCM anion	gp complex	C-PCM complex	gp cresol
19a	1501	1560	1519	1548	1521	1551
$\Delta\nu$	0[a]	−13	−4	−8	−2	−1
7a	1267	1411	1348	1395	1321	1284
$\Delta\nu$	−17[a]	−13	−19	−16	−19	−11

B. ^{13}C Shifts for *para*-Cresol

ν	experiment	gp anion	C-PCM anion	gp complex	C-PCM complex	gp cresol
8a	1606[a]	1640	1636	1643	1638	1660
$\Delta\nu(^{13}C_6)$[b]		−55	−55	−56	−55	−57
$\Delta\nu(^{13}C_1)$[c]		−6	−2	−4	−2	−5
19a	1501[a]	1560	1519	1548	1521	1551
$\Delta\nu(^{13}C_6)$		−40	−37	−38	−36	−37
$\Delta\nu(^{13}C_1)$		−23	−13	−19	−11	−9
7a	1268[a]	1411	1348	1395	1321	1284
$\Delta\nu(^{13}C_6)$		−29	−30	−29	−31	−31
$\Delta\nu(^{13}C_1)$		−10	−23	−15	−24	−24
9a	1173[a]	1193	1195	119	1198	1214
$\Delta\nu(^{13}C_6)$		−11	−12	−11	−11	0
$\Delta\nu(^{13}C_1)$		0	0	0	−1	−1

C. ^{2}H Shifts for *para*-Cresol

ν	experiment	gp anion	C-PCM anion	gp complex	C-PCM complex	gp cresol
8a	1606	1640	1636	1643	1638	1660
$\Delta\nu(^{2}H_4)$[d]	−30[f]	−31	−34	−32	−33	−30
$\Delta\nu(^{2}H_2)$[e]	−11[f]	−10	−7	−10	−7	−11
19a	1501	1560	1519	1548	1521	1551
$\Delta\nu(^{2}H_4)$	−75[f]	−34	−68	−46	−79	−90
$\Delta\nu(^{2}H_2)$	−40[f]	−18	−40	−27	−47	−44
7a	1268	1411	1348	1395	1321	1284
$\Delta\nu(^{2}H_4)$	−30[a]	−84	−49	−72	−38	−35
$\Delta\nu(^{2}H_2)$	−6[a]	−31	−10	−23	−5	−−9
9a	1173	1193	1195	119	1198	1214
$\Delta\nu(^{2}H_4)$	−319[f]	−363	−362	−347	−363	−368
$\Delta\nu(^{2}H_2)$	−112[f]	−134	−134	−131	−133	−143

[a] Difference FTIR, pH 12.23 [b] Ring atoms substituted with ^{13}C. [c] C_i isotopically substituted with ^{13}C. [d] Ring atoms substituted with ^{2}H. [e] H_o and H_o' isotopically substituted with ^{2}H. [f] FTIR, 50 mM cresol in carbon disulfide and dichloroethene;[39] gp = gas-phase.

TABLE 9: UB3LYP/6-31+G(d,p) Calculated Bond Lengths (Å) and Angles (°) for the Phenoxyl Radical

	gas-phase radical	C-PCM radical[a]	gas-phase radical complex[b]	C-PCM radical complex[c]
$R(OH_1)$			1.891	1.836
$R(OC_i)$	1.261	1.266	1.263	1.269
$R(C_oC_i)$	1.454	1.454	1.452	1.452
$R(C_mC_o)$	1.380	1.379	1.380	1.379
$R(C_pC_m)$	1.412	1.414	1.413	1.415
$A(OC_iC_o)$	121.3	121.2	121.1	121.0
$A(C_o'C_iC_o)$	117.4	117.6	117.8	118.0
$A(C_iC_oC_m)$	120.7	120.6	120.4	120.4
$A(C_oC_mC_p)$	120.3	120.2	120.3	120.2
$A(C_m'C_pC_m)$	120.7	120.8	120.8	120.8

[a] C-PCM water-solvated phenoxyl radical. [b] Gas-phase phenoxyl−H_2O radical complex. [c] C-PCM water-solvated phenoxyl−H_2O radical complex.

TABLE 10: Observed and Calculated Fundamental Frequencies (in cm^{-1}) for the Phenoxyl Radical

Wilson mode	observed[a]	gas-phase radical	C-PCM radical	gas-phase complex	C-PCM complex
8a	1557	1589	1589	1597	1598
7a	1505	1489	1504	1510	1517
19a	1398	1419	1417	1430	1425
9a	1163	1170	1170	1173	1168
18a	990	976	976	991	991
1	801	805	808	818	821
6a	528	527	527	541	542

[a] UV−resonance Raman, 245 nm excitation, 0.1 M NaOH.[21]

has a smaller impact on the neutral radical structure than on the negatively charged anion. While the anion OC_i bond length increases by 3.5 pm from the gas phase to the C-PCM water-solvated complex, the radical bond length increases by only 0.8 pm. In addition, the anion C_oC_i bonds shorten by 2.1 pm from the gas phase to the C-PCM water-solvated complex, while these bonds are decreased by only 0.27 pm for the radical. The consistently short OC_i bonds, long C_oC_i bonds, and narrow $C_o'C_iC_o$ angles suggest a highly quinoidal radical structure.

Observed and calculated vibrational frequencies for the phenoxyl radical appear in Table 10. The complete set of calculated frequencies is given in Table S6 of the Supporting Information. Agreement between theory and experiment is better for the neutral radical than that for the anion, with mean absolute errors of 14.0 (1.05%), 11.6 (0.94%), 16.8 (1.53%), and 17.1 cm^{-1} (1.57%) for the gas-phase radical, C-PCM water-solvated radical, gas-phase phenoxyl−H_2O radical complex, and C-PCM water-solvated phenoxyl−H_2O radical complex, respectively. As with the anion, the C-PCM water-solvated radical yields

TABLE 11: Observed and Calculated Isotope Shifts (in cm^{-1})

A. ^{17}O Shifts for Phenoxyl Radical

ν	experiment[a]	gp radical	C-PCM radical	gp complex	C-PCM complex
7a	1505	1489	1504	1510	1517
$\Delta\nu$	−13	−6	−8	−7	−8
19a	1398	1419	1417	1430	1425
$\Delta\nu$	−30	−8	−7	−8	−7

B. ^{13}C Shifts for Phenoxyl Radical

ν	experiment	gp radical	C-PCM radical	gp complex	C-PCM complex
8a	1557	1589	1589	1597	1598
$\Delta\nu(^{13}C_6)$[b]	−52[a]	−51	−53	−53	−54
$\Delta\nu(^{13}C_1)$[c]	0[d]	0	0	0	0
7a	1505	1489	1504	1510	1517
$\Delta\nu(^{13}C_6)$	−36[a]	−35	−37	−37	−37
$\Delta\nu(^{13}C_1)$	−26[d]	−22	−26	−23	−26
19a	1398	1419	1417	1430	1425
$\Delta\nu(^{13}C_6)$	−23[a]	−25	−24	−26	−25
$\Delta\nu(^{13}C_1)$	−16[d]	−14	−11	−13	−12
9a	1163	1170	1170	1173	1168
$\Delta\nu(^{13}C_6)$	−8[a]	−8	−7	−8	−6
$\Delta\nu(^{13}C_1)$		−1	0	−1	0

C. ^{2}H Shifts for Phenoxyl Radical

ν	Experiment	gp radical	C-PCM radical	gp complex	C-PCM complex
8a	1557	1589	1589	1597	1598
$\Delta\nu(^{2}H_5)$[e]	−44[a]	−44	−45	−44	−42
$\Delta\nu(^{2}H_3)$[f]		−10	−12	−11	−13
7a	1505	1489	1504	1510	1517
$\Delta\nu(^{2}H_5)$	−15[a]	−32	−24	−29	−24
$\Delta\nu(^{2}H_3)$	−18[g]	−31	−23	−29	−22
19a	1398	1419	1417	1430	1425
$\Delta\nu(^{2}H_5)$	−153[h]	−158	−163	−155	−155
$\Delta\nu(^{2}H_3)$		−38	−41	−40	−41
9a	1163	1170	1170	1173	1168
$\Delta\nu(^{2}H_5)$	−298[a]	−325	−328	−326	−326
$\Delta\nu(^{2}H_3)$	−100[g]	−97	−103	−96	−98

[a] UV−resonance Raman, 245 nm excitation, 0.1 M NaOH.[21] [b] Ring atoms isotopically substituted with ^{13}C. [c] C_i isotopically substituted with ^{13}C. [d] FT- IR, Ar matrix.[20] [e] H atoms isotopically substituted with ^{2}H. [f] H_o, H_o', and H_p isotopically substituted with ^{2}H. [g] UV−resonance Raman, 399 nm excitation, pH 11.[22] [h] FT-IR, Ar matrix;[20] gp = gas-phase.

overall the most accurate results. The C-PCM shifts mode 7a up by 15 cm^{-1} from the gas-phase radical, and agreement with experiment is excellent. The gas-phase phenoxyl−H_2O radical complex shifts this mode in the correct direction, albeit overshooting the mark, as does the C-PCM water-solvated phenoxyl−H_2O radical complex.

Observed and calculated isotope shifts for the phenoxyl radical are listed in Table 11A−C. Agreement between theory and experiment is better for the radical than that for the anion. However, some large deviations do occur; the ^{17}O shifts are consistently underestimated, and as previously described,[14,22,23] the calculated gas-phase mode 7a ^{2}H shifts are roughly twice the observed shift. It should be noted that for the C-PCM water-solvated structures, the mode 7a ^{2}H shifts are smaller and in better agreement with experiment. For the radical, as with the anion, a large ^{2}H shift is observed for 19a, and a much smaller shift is observed for mode 7a. This pattern is predicted by all solvation models, and the calculated mode 19a shifts are in good agreement with experiment.

***para*-Cresol Radical.** Selected structural parameters for *para*-cresol radical are listed in Table 12. The atom label definitions are those defined in Figure 2. The complete set of calculated structural parameters appears in Table S7 of the Supporting Information. The predicted structure of the *para*-cresol radical does not differ significantly from that of the phenoxyl radical. The largest structural change is an increased O_{water}−O distance (not shown; see Table S7 of the Supporting Information) of 4 pm for the C-PCM water-solvated *para*-cresol-H_2O radical complex compared to that of the C-PCM water-solvated phenoxyl−H_2O radical complex. The *para*-cresol $C_m'C_pC_m$

TABLE 12: UB3LYP/6-31+G(d,p) Calculated Bond Lengths (Å) and Angles (°) for *para*-Cresol Radical

	gas-phase radical	C-PCM radical[a]	gas-phase complex[b]	C-PCM complex[c]
$R(OH_1)$			1.899	1.877
$R(OC_i)$	1.260	1.267	1.264	1.271
$R(C_oC_i)$	1.453	1.453	1.452	1.451
$R(C_mC_o)$	1.377	1.376	1.377	1.376
$R(C_pC_m)$	1.419	1.422	1.419	1.422
$A(OC_iC_o)$	121.7	121.5	121.3	121.3
$A(C_o'C_iC_o)$	116.6	116.9	117.4	117.4
$A(C_iC_oC_m)$	121.0	120.9	120.6	120.7
$A(C_oC_mC_p)$	121.5	121.4	121.3	121.2
$A(C_m'C_pC_m)$	118.5	118.5	118.9	118.8

[a] C-PCM water-solvated *para*-cresol radical. [b] Gas-phase *para*-cresol−H_2O radical. [c] C-PCM water-solvated *para*-cresol−H_2O radical.

TABLE 13: Observed and Calculated Fundamental Frequencies in cm^{-1} for *para*-Cresol Radical

Wilson mode	observed[a]	gas-phase radical	C-PCM radical	gas-phase complex	C-PCM complex
8a	1577	1607	1608	1613	1617
7a	1517	1502	1519	1525	1522
19a	1407	1433	1431	1437	1431
9a	1161	1183	1185	1176	1176
18a	980	983	975	1001	977
1	817	816	820	825	828

[a] UV−resonance Raman, 406 nm excitation, KOH; J. Phys. Chem. 1988, 92, 5129−5133.

angle is also 2° smaller than that in the corresponding phenoxyl radical structures. The remaining equivalent ring bonds are changed by less than 1 pm and angles by less than 1°.

Observed and calculated fundamental frequencies for the *para*-cresol radical are listed in Table 13. The complete set of calculated frequencies appears in Table S8 of the Supporting Information. The mean absolute errors of 16.1 (1.17%), 14.7 (1.12%), 19.7 (1.56%), and 16.1 cm^{-1} (1.23%) for the gas-phase radical, C-PCM radical, gas-phase complex, and C-PCM complex, respectively, are slightly larger than was observed for the phenoxyl radical; however, these are considerably smaller than the errors associated with the *para*-cresolate anion. The C-PCM water-solvated radical provides the best agreement between theory and experiment. As was observed for the phenoxyl radical, Wilson mode 7a is underestimated by the gas-phase structure, and the C-PCM shifts this mode to higher energy, providing remarkable agreement with experiment. As was observed for the phenoxyl radical, this frequency is slightly overestimated by the H-bonded models.

Table 14A−C compares calculated and observed isotope shifts for the *para*-cresol radical. Few isotope shifts have been assigned. From Table 14A, the gas-phase radical mode 7a ^{18}O shift is underestimated, but this shift is improved with the solvation models. The predicted mode 19a ^{18}O shifts are similar to the predicted shifts of the phenoxyl radical, and it is expected that these shifts are likewise underestimated. The calculated ^{2}H shifts for mode 7a are overestimated, and solvation provides significant improvements.

Vibrational Projection Analysis of Wilson Modes 7a and 19a. Vibrational projection analysis[36] was performed to provide a quantitative comparison of the anion and the radical normal coordinates. For phenol, the radical and anion modes 8a and 9a overlap coefficients are large (∼0.8) for all structures, although the gas-phase phenoxyl radical mode 8a is a mixture of the anion 8a and 19a modes. The projection coefficients for modes 18a, 1, and 6a are smaller (∼0.5−0.6); however, the analysis supports the current assignment because these are the largest overlap coefficients and the only coefficients that overlap frequencies within several hundred wavenumbers.

The analysis for phenoxyl radical modes 7a and 19a is much less straightforward. The projection coefficients of the radical modes using the anion modes as a basis appear in Table 15A. It is clear that for the gas-phase phenoxyl radical and gas-phase phenoxyl−H_2O radical complex, the radical mode labeled 7a has a larger overlap with the anion mode 19a (0.708 and 0.687, respectively), and the radical mode 19a has a larger overlap with the anion mode 7a (0.623 and −0.586, respectively). For the C-PCM water-solvated radical and C-PCM water-solvated phenoxyl−H_2O radical complex, the radical mode 7a is a symmetric combination of anion modes 19a and 7a, and the radical mode 19a is an asymmetric combination of anion modes 19a and 7a. The projection coefficients of the phenolate anion modes using the radical modes as a basis appear in Table 15B. For all of the structures, the anion mode 7a has a larger overlap with the radical mode 19a than with the radical mode 7a, and the anion mode 19a has a larger overlap with the radical mode 7a than with the radical mode 19a. In addition, there is much less mixing of the radical modes 7a and 19a into the anion modes 7a and 19a for the C-PCM water-solvated structures.

Vibrational projection analysis[37] was performed to quantitatively compare the radical and anion normal coordinates for *para*-cresol. For all of the structures, the 8a projection coefficients are large (∼0.8), allowing an unambiguous assignment. The projection coefficients of the radical modes 7a and 19a using the anion modes as a basis are listed in Table 16A, while the coefficients for the anion modes 7a and 19a using the radical modes as a basis are listed in Table 16B. The results from Table 16A and B are similar to those of the phenoxyl radical, and similar conclusions may be drawn regarding the assignment of modes 7a and 19a.

Total Energy Decomposition of Wilson Modes 7a and 19a. The total energy decomposition[45] for phenolate Wilson modes 7a and 19a appears in Table 17A, while the decomposition for the phenoxyl radical modes appears in Table 17B. It is clear from Table 17A that the phenolate modes 7a are dominated by C_iO stretching for all solvation models, while the gas-phase anion predicts more C_iO stretching in mode 19a than in 7a. A similar energy distribution occurs in the gas-phase complex, although correctly, there is a larger contribution of C_iO stretching in mode 7a. While the energy distribution of the gas-phase anions is incorrect, it is easily understood. The gas-phase anion and phenolate-H_2O complex predict a short, strong C_iO bond with significant double-bond character. For the gas-phase anion, the intrinsic C_iO frequency[46] is 1423 cm^{-1}, while this stretch is 1293, 1378, 1270, and 1145 cm^{-1} in the C-PCM water-solvated anion, gas-phase phenolate−H_2O complex, C-PCM water-solvated phenolate−H_2O complex, and gas-phase phenol, respectively. The large intrinsic frequencies of the gas-phase anionic C_iO stretch results in a larger C_iO stretching contribution in the higher-energy Wilson modes 19a, which is supported by the isotope shifts (see Table 3A). It should also be noted that for the gas-phase anionic structures, there is nearly twice as much total CH bending in mode 7a compared to either that of the C-PCM water-solvated structures or that of the gas-phase phenol, consistent with the large calculated ^{2}H isotope shifts (see Table 3C). For mode 19a, there is a systematic decrease in the C_iO stretching contribution as the solvation model is improved, while the contributions from the other internal motions are relatively consistent across solvation models. A comparison of both the C-PCM water-solvated phenolate anions and the gas-phase phenol total energy distributions reveals that mode 7a of both of the C-PCM water-solvated structures may be interpreted as the C_iO stretch, whereas the O-protonated structure includes a larger contribution from C_oC_i stretching.

It is clear from Table 17B that the phenoxyl radical mode labeled 7a is likewise dominated by C_iO stretching, and the phenoxyl radical mode 19a has larger total contributions from CH bending. A comparison of the radical and anion mode 7a, however, reveals that the anion mode 7a contains significant C_mC_o stretching, while the radical mode 7a contains significant C_oC_i stretching and a small contribution from C_pC_m stretching. However, the anion mode 19a contains large contributions from C_oC_i and C_pC_m stretching, while the radical mode 19a contains contributions from C_pC_m stretching.

TABLE 14: Observed and Calculated Isotopes (in cm^{-1})

A. ^{18}O Shifts for *para*-Cresol Radical

ν	experiment[a]	gp radical	C-PCM radical	gp complex	C-PCM complex
7a	1513	1502	1519	1525	1529
$\Delta\nu$	−15	−9	−13	−11	−14
19a	1407	1433	1431	1437	1431
$\Delta\nu$		−17	−15	−15	−15

B. ^{13}C Shifts for *para*-Cresol Radical

ν	experiment[b]	gp radical	C-PCM radical	gp complex	C-PCM complex
8a	1577	1607	1608	1613	1617
$\Delta\nu(^{13}C_6)$[c]		−51	−53	−54	−53
$\Delta\nu(^{13}C_1)$[d]		0	0	0	0
7a	1513	1502	1519	1525	1529
$\Delta\nu(^{13}C_6)$		−38	−38	−38	−41
$\Delta\nu(^{13}C_1)$		−21	−26	−23	−26
19a	1407	1433	1431	1437	1431
$\Delta\nu(^{13}C_6)$		−26	−26	−32	−28
$\Delta\nu(^{13}C_1)$		−14	−11	−13	−12
9a	1161	1170	1170	1173	1168
$\Delta\nu(^{13}C_6)$		−8	−7	−8	−7
$\Delta\nu(^{13}C_1)$		−1	0	−1	−1

C. ^{2}H Shifts for *para*-Cresol Radical

ν	experiment[a]	gp radical	C-PCM radical	gp complex	C-PCM complex
8a	1577	1607	1608	1613	1617
$\Delta\nu(^{2}H_4)$[e]		−41	−41	−35	−37
$\Delta\nu(^{2}H_2)$[f]		−8	−9	−10	−12
7a	1513	1502	1519	1525	1529
$\Delta\nu(^{2}H_4)$	−20	−32	−23	−30	−25
$\Delta\nu(^{2}H_2)$	−15	−31	−22	−29	−20
19a	1407	1433	1431	1437	1431
$\Delta\nu(^{2}H_4)$		−106	−109	−95	−96
$\Delta\nu(^{2}H_2)$		−26	−24	−31	−31
9a	1161	1170	1170	1173	1168
$\Delta\nu(^{2}H_4)$		−331	−335	−319	−323
$\Delta\nu(^{2}H_2)$		−126	−128	−113	−117

[a] Difference FT-IR, pH 12.[23] [b] UV−resonance Raman, 406 nm excitation, KOH (J. Phys. Chem. 1988, 92, 5129−5133). [c] Ring atoms isotopically substituted with ^{13}C. [d] C_i isotopically substituted with ^{13}C. [e] Ring atoms isotopically substituted with ^{2}H. [f] H_o and H_o' isotopically substituted with ^{2}H; gp = gas-phase.

TABLE 15: Projection Analysis Coefficients for Phenol

A. Radical Modes on Anion Modes

		gas-phase radical		C-PCM radical		gas-phase radical complex		C-PCM radical complex	
		7a	19a	7a	19a	7a	19a	7a	19a
anion	7a	−0.262 (6.9%)	0.623 (39%)	0.670 (45%)	−0.473(22%)	0.426 (18%)	−0.586 (34%)	0.680 (46%)	−0.451 (20%)
	19a	0.708 (50%)	0.178 (3.2%)	0.671 (45%)	0.428(18%)	0.687 (47%)	0.284 (8.1%)	0.606 (37%)	0.452 (20%)

B. Anion Modes on Radical Modes

		gas-phase anion		C-PCM anion		gas-phase anion complex		C-PCM anion complex	
		7a	19a	7a	19a	7a	19a	7a	19a
radical	7a	0.172(3.0%)	0.604(36%)	0.212(4.5%)	0.818 (67%)	−0.046(0.21%)	0.702 (49%)	0.275(7.6%)	0.785 (62%)
	19a	0.612 (37%)	−0.398(16%)	−0.719 (52%)	−0.136(1.8%)	−0.656 (43%)	−0.283(8.0%)	−0.732 (54%)	−0.082(0.67%)

The total energy decomposition for the *para*-cresolate anion and the *para*-cresol radical appears in Table 18A and B, respectively. The analysis for the *para*-cresol anion and radical parallels that for phenol, that is, mode 7a is dominated by C_iO stretching, while mode 19a contains large total contributions from CH bending motions. As with the phenol anion and radical, the *para*-cresolate anion mode 7a contains significant C_mC_o stretching, the anion mode 19a includes significant contributions from C_oC_i and C_pC_m stretching, and the *para*-cresol radical mode 7a contains significant C_oC_i stretching with a small contribution from C_pC_m stretching, while the *para*-cresol radical mode 19a includes C_pC_m stretching. In contrast to the phenoxyl radical, the *para*-cresol radical mode 19a has more total energy from C_mC_o stretching than from C_pC_m stretching.

On the basis of the energy distribution of the C_iO stretch and CH bending motions, one may conclude that the current assignment of the radical and anion modes is consistent, that is, mode 7a has a larger C_iO stretching contribution than 19a,

TABLE 16: Projection Analysis Coefficients for *para*-Cresol

a. Radical Modes on Anion Modes

		gas-phase radical		C-PCM radical		gas-phase radical complex		C-PCM radical complex	
		7a	19a	7a	19a	7a	19a	7a	19a
anion	7a	−0.202 (4.1%)	0.697 (49%)	0.644 (41%)	−0.465 (22%)	0.326 (11%)	−0.595 (35%)	0.488 (24%)	−0.406 (16%)
	19a	0.801 (64%)	0.126 (1.6%)	0.715 (51%)	0.412 (17%)	0.583 (34%)	0.215 (4.6%)	0.542 (29%)	0.427 (18%)

B. Anion Modes on Radical Modes

		gas-phase anion		C-PCM anion		gas-phase anion complex		C-PCM anion complex	
		7a	19a	7a	19a	7a	19a	7a	19a
radical	7a	0.121 (1.5%)	0.752 (57%)	0.296 (8.8%)	0.842 (71%)	0.019 (0.04%)	0.686 (47%)	0.291 (8.5%)	0.696 (48%)
	19a	0.725 53%)	−0.282 (8.0%)	−0.711 (51%)	0.055 (0.3%)	−0.653 (43%)	−0.156 (2.4%)	−0.657 (43%)	0.138 (1.9%)

TABLE 17: Total Energy Decomposition (%)

A. Phenolate Anion

		gas-phase anion	C-PCM anion	gas-phase complex	C-PCM complex	gas-phase phenol
19a	C_iO	43.20	19.19	32.84	13.48	5.86
	C_oC_i	4.69	12.91	9.47	14.74	12.08
	C_mC_o	8.80	0.01	3.01	0.15	4.78
	C_pC_m	11.50	10.74	12.11	11.47	14.04
	H_o bend	7.68	27.36	16.10	29.59	19.18
	H_m bend	18.63	23.24	20.25	24.08	31.11
	H_p bend	8.97	0.56	0.82	0.59	2.17
7a	C_iO	29.43	59.62	43.95	63.35	52.65
	C_oC_i	2.40	0.00	0.59	0.17	6.33
	C_mC_o	10.28	9.05	10.47	8.77	12.74
	C_pC_m	4.59	1.22	3.22	0.87	0.57
	H_o bend	28.24	12.24	21.00	9.37	9.50
	H_m bend	22.01	12.26	16.45	10.30	8.65
	H_p bend	0.01	0.08	0.10	0.15	0.41

B. Phenoxyl Radical

		gas-phase radical	C-PCM radical	gas-phase complex	C-PCM complex
19a	C_iO	37.28	31.08	37.21	33.51
	C_oC_i	1.13	1.43	1.14	1.32
	C_mC_o	3.47	3.84	3.41	3.66
	C_pC_m	4.83	5.41	5.22	5.77
	H_o bend	16.06	21.30	18.08	21.40
	H_m bend	33.26	33.43	30.50	30.15
	H_p bend	0.07	0.06	0.09	0.05
7a	C_iO	45.78	55.49	47.30	53.14
	C_oC_i	6.58	6.97	8.02	8.21
	C_mC_o	2.46	0.27	1.90	0.00
	C_pC_m	2.47	2.80	2.96	3.99
	H_o bend	30.17	21.35	26.87	19.71
	H_m bend	4.68	5.96	5.46	8.00
	H_p bend	0.02	0.09	0.13	0.23

and 19a has a larger CH bending contribution than 7a. However, this may be misleading because the potential energy distribution does not contain phasing information with respect to the individual stretching and bending motions. The most important information for distinguishing modes 7a and 19a is the phasing of the C_iO and the C_iC_o stretches. The calculated atomic displacements[47] for the C-PCM water-solvated phenolate anion and phenoxyl radical modes 7a and 19a appear in Figure 3. Figure 3A shows that the anion mode 7a is a symmetric combination of the C_iO and the C_iC_o bond stretches, while Figure 3B shows that mode 19a is an asymmetric combination of the C_iO and the C_iC_o bond stretches. However, it is clear from Figure 3C that the radical mode 7a is an asymmetric combination of C_iO and C_iC_o stretching, while Figure 3D shows that the radical mode 19a is a symmetric combination of these stretches. In this regard, the vibrational projection analysis discussed in the previous section is more informative and correctly correlates the radical mode 19a to the closed-shell 7a and vice versa. The high-energy C_iO intrinsic frequencies of 1401, 1409, 1414, and 1413 cm^{-1} for the gas-phase phenoxyl radical, C-PCM water-solvated phenoxyl radical, gas-phase phenoxyl−H_2O radical complex, and C-PCM water-solvated phenoxyl−-H_2O radical complex, respectively, are similar to that of the gas-phase anion and suggests a similar interpretation. The high-energy nature of this stretch is mixed into mode 19a, and thus, it may be incorrect to assign mode 7a to that normal coordinate with the largest contribution of C_iO stretching.

These results suggest that the relative phasing of the C_iO and C_iC_o stretches may be an alternative criterion for distinguishing between modes 7a and 19a. There are two possibilities; one could choose mode 7a to be the symmetric and 19a to be the asymmetric C_iO and C_iC_o stretching mode, or one could choose

TABLE 18: Total Energy Decomposition (%)

A. *para*-Cresolate Anion

		gas-phase anion	C-PCM anion	gas-phase complex	C-PCM complex	gas-phase *p*-cresol
19a	C_iO	40.69	13.85	21.95	9.61	5.95
	C_oC_i	8.93	15.52	13.32	15.63	15.85
	C_mC_o	0.60	2.89	0.07	2.71	0.29
	C_pC_m	10.56	8.40	18.24	8.96	12.20
	H_o bend	13.28	29.94	16.93	32.37	27.34
	H_m bend	15.77	19.10	16.20	20.46	27.80
7a	C_iO	36.24	62.89	47.16	61.86	50.28
	C_oC_i	1.56	0.15	0.14	0.80	6.61
	C_mC_o	18.03	11.91	15.78	11.22	16.08
	C_pC_m	2.69	0.38	1.90	0.65	0.27
	H_o bend	21.55	7.62	14.52	6.75	5.79
	H_m bend	15.78	9.35	12.24	10.48	11.97

B. *para*-Cresol Radical

		gas-phase radical	C-PCM radical	gas-phase complex	C-PCM complex
19a	C_iO	38.01	32.79	36.85	34.69
	C_oC_i	1.22	1.26	1.07	1.17
	C_mC_o	8.01	8.66	6.39	7.56
	C_pC_m	4.22	4.79	6.77	6.90
	H_o bend	12.25	16.62	16.26	17.76
	H_m bend	30.58	30.09	24.06	24.35
7a	C_iO	41.43	52.14	45.90	41.12
	C_oC_i	7.49	7.97	8.17	9.26
	C_mC_o	5.64	1.10	2.54	4.14
	C_pC_m	2.60	3.11	3.26	5.48
	H_o bend	28.50	20.25	25.80	19.02
	H_m bend	3.75	6.46	4.47	7.00

mode 7a to be the asymmetric and 19a to be the symmetric C_iO and C_iC_o stretching mode. With the former possibility, the current assignment of the anion modes 7a and 19a is unchanged; however, the radical modes 7a and 19a are not unique but are a symmetric and asymmetric combination of the anion modes 7a and 19a, respectively (see Tables 15A and 16A, projection analysis). However, if mode 7a is the asymmetric and 19a is the symmetric C_iO and C_iC_o stretching mode, then the current assignment of the radical modes 7a and 19a is unchanged, the anion mode 7a should be relabeled mode 19a, and the anion mode 19a should be relabeled 7a. However, the anion modes 7a and 19a are not combinations of radical modes 7a and 19a, and there would then be one-to-one correspondence between the radical and anion mode 7a and between the radical and anion mode 19a.

Conclusions

The effects of aqueous solvation on the structure and vibrational frequencies of phenol, *para*-cresol, and their respective radicals were explored at the B3LYP/6-31+G(d,p) level of theory. Solvation was included using the electrostatic conductor-like polarizable continuum model (C-PCM) alone and by including one explicit water molecule H-bonded to the phenolic oxygen. None of the models investigated in this study are able to reproduce all of the experimental frequencies and isotope shifts. However, the C-PCM provides the best overall agreement between theory and experiment at a modest computational effort, except for the anionic Wilson mode 7a frequency, which is correctly predicted by the gas-phase oxygen-protonated structures and is overestimated by the remaining solvation models. For phenolate and *para*-cresolate anions, the electrostatic interactions between the solute and solvent are dominant, and the gas-phase H-bonded complexes do not provide significant improvements over the gas-phase anion structures. The X3LYP and PBE0 functionals provide tighter binding between the anion and water molecules, as demonstrated by the calculated structures, but fail to improve the predicted vibrational frequencies. For the neutral radical structures, solvation has a smaller impact on the computed frequencies, and the gas-phase models provide reasonable results. Inclusion of the C-PCM shifts important frequencies to higher energy, providing frequencies in excellent agreement with experiment.

Regarding the anion Wilson mode 7a, which is generally assigned to the C−O stretch, an electrostatic model of solvation fails to predict the 7a frequency with the same accuracy as the O-protonated structure; however, the conductor-like polarizable continuum model provides the best compromise with regards to overall accuracy, as demonstrated by the mean absolute errors in the computed frequencies. The gas-phase phenol and *para*-cresol structures underestimate the ^{18}O isotope shifts, while the C-PCM water-solvated models correctly predict this important isotope shift.

Wilson mode 7a, interpreted as the C−O stretch, has been observed at 1266 cm^{-1} for tyrosine residues in aqueous base at cryogenic temperatures,[14] in excellent agreement with the 1264 cm^{-1} frequency observed in the resonance Raman spectrum of phenol in aqueous NaOH.[15] As there is no mention of cryogenic temperatures in ref 15, one must assume this measurement is conducted at ambient temperature. Because the 7a vibration is observed at the same frequency as that in the polycrystalline phase, it must be concluded that the molecular interactions between solute and solvent are the same in both phases. The Raman study of Takeuchi et al.[36] explored the effects of H-bonding on *para*-cresol and crystalline tyrosine residues and dipeptides. The observed bands assigned to mode 7a ranged from 1255 to 1272 cm^{-1} for *para*-cresol in a variety of solvents. The highest energy band of 1272 cm^{-1} was observed with

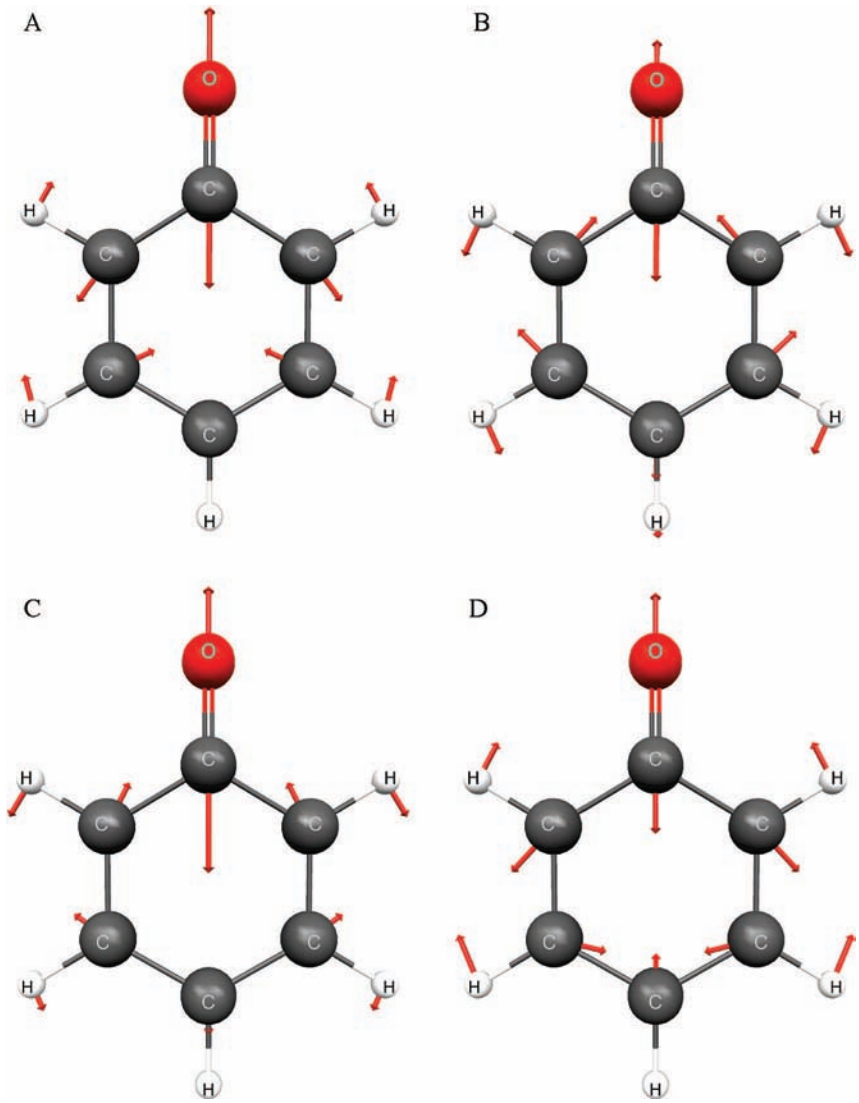

Figure 3. Calculated atomic displacements for (A) C-PCM water-solvated anion mode 7a, (B) C-PCM water-solvated anion mode 19a, (C) C-PCM water-solvated radical mode 7a, and (D) C-PCM water-solvated radical mode 19a.

triethylamine as the solvent, while in H_2O at pH 13, this mode was observed at 1266 cm^{-1}. In the case of crystalline tyrosine residues and dipeptides, mode 7a is observed at 1259−1265 cm^{-1}, and in a nonpolar Nujol mull,[48] this stretch occurs at 1212 cm^{-1}. If the calculated frequency of 1321 cm^{-1} obtained with the C-PCM water-solvated complex (Table 7) is considered an upper limit to the C−O stretch, then the narrow range of 1212−1272 cm^{-1} demonstrates that phenol is reluctant to give up its proton and maintains a very strong O−H bond, even with powerful H-bond acceptors like triethylamine and hydroxide; thus, an updated chemical picture of the phenol deprotonation is needed.

Our vibrational projection analysis data, when combined with the total energy decomposition analysis, suggest that the low-energy anion mode 7a may be interpreted as the C_iO stretch and the high-energy anion mode 19a as CH bending and C_oC_i stretching, with a small contribution from C_iO stretching. In the radical, by contrast, the intrinsic frequency of the C_iO stretch increases, and this stretch contributes to both the 7a and 19a radical modes. By comparing the phasing of the individual C_iO and C_iC_o stretches, we showed that mode 7a is currently a symmetric combination of these bond stretches and that the 19a is an asymmetric combination. This offers an alternative interpretation of modes 7a and 19a. If mode 7a remains the symmetric and 19a remains the asymmetric combination of C_iO and C_iC_o stretches, then the current definition of anion modes 7a and 19a is retained. Consequently, the radical mode 7a is better described as a symmetric combination of the anion modes 7a and 19a, and the radical mode 19a is an asymmetric combination of anion modes 7a and 19a. This means there is no unique radical mode 7a or 19a. Conversely, if mode 7a is the asymmetric and 19a is the symmetric C_iO and C_iC_o stretching mode, then the current assignment of the radical modes 7a and 19a is retained, and the anion mode 7a should be relabeled 19a and the anion mode 19a relabeled 7a. As the *para*-cresolate anion is a suitable model for the tyrosinate anion, these results suggest that the same interpretation applies to the tyrosinate and tyrosyl radical modes.

Acknowledgment. This work was supported by National Institutes of Health Grant GM53788.

Supporting Information Available: Optimized internal coordinates and all calculated frequencies for phenol, *para*-cresol, phenoxyl radical, and *para*-cresol radical. This material is available free of charge via the Internet at http://pubs.acs.org.

References and Notes

(1) Barry, B. A.; Babcock, G. T. *Proc. Natl. Acad. Sci. U.S.A.* **1987**, *84*, 7099–7103.

(2) Pujois-Ayala, I.; Barry, B. A. *Biochim. Biophys. Acta* **2004**, *1655*, 205–216.

(3) Ostreimer, C.; Harrenga, A.; Ermler, U.; Michel, H. *Proc. Natl. Acad. Sci. U.S.A.* **1997**, *94*, 10547–10553.

(4) Yoshikawa, S.; Shinzawa-Itoh, K.; Nakashima, R.; Yaono, R.; Yamashita, E.; Inoue, N.; Yao, M.; Fei, M. J.; Libeu, C. P.; Mizushima, T.; Yamaguchi, H.; Tomizaki, T.; Tsukihara, T. *Science* **1998**, *280*, 1723–1729.

(5) Larsson, A.; Sjoberg, B.-M. *EMBO J.* **1986**, *5*, 2037–2040.

(6) Smith, W. L.; Eling, T. E.; Kulmacz, R. J.; Marnett, L. J.; Tsai, A.-L. *Biochemistry* **1992**, *31*, 3–7.

(7) Whittaker, M. M.; Whittaker, J. W. *J. Biol. Chem.* **1990**, *265*, 9610–9613.

(8) Silva, K. E.; Elgren, T. E.; Que, L., Jr.; Stankovich, M. T. *Biochemistry* **1995**, *34*, 14093–14103.

(9) Cappuccio, J. A.; Ayala, I.; Elliott, G. I.; Szundi, I.; Lewis, J.; Konopelski, J. P.; Barry, B. A.; Einarsdóttir, Ó. *J. Am. Chem. Soc.* **2002**, *124*, 1751–1760.

(10) See, for example: Berthomieu, C.; Heinerwadel, R. *Biochim. Biophys. Acta* **2005**, *1707*, 51–66, and references therein.

(11) Hill, B. C.; Greenwood, C. *Biochem. J.* **1984**, *218*, 913–921.

(12) Varotsis, C.; Zhang, Y.; Appelman, E. H.; Babcock, G. T. *Proc. Natl. Acad. Sci. U.S.A.* **1993**, *90*, 237–241.

(13) Morgan, J. E.; Verkhovsky, M. I.; Wikström, M. *Biochemistry* **1996**, *35*, 12235–12240.

(14) Karpefors, M.; Ädelroth, P.; Aagaard, A.; Sigurdson, H.; Ek, M. S.; Brzezinski, P. *Biochim. Biophys. Acta* **1998**, *1365*, 159–169.

(15) Sucheta, A.; Szundi, I.; Einarsdóttir, Ó. *Biochemistry* **1998**, *37*, 17905–17914.

(16) (a) Einarsdóttir, Ó.; Szundi, I. *Biochim. Biophys. Acta* **2004**, *1655*, 263–273. (b) Van Eps, V.; Szundi, I.; Einarsdóttir, Ó. *Biochemistry* **2003**, *42*, 5065–5073.

(17) (a) DeGray, J. A.; Lassmann, G.; Curtis, J. F.; Kennedy, T. A.; Marnett, L. J.; Eling, T. E.; Mason, R. P. *J. Biol. Chem.* **1992**, *267*, 23583–23588. (b) Hoganson, C. W.; Babcock, G. T. *Biochemistry* **1992**, *31*, 11874–11880.

(18) Johnson, C. R.; Ludwig, M.; Asher, S. A. *J. Am. Chem. Soc.* **1986**, *108*, 905–912.

(19) Range, K.; Ayala, I.; York, D.; Barry, B. A. *J. Phys. Chem. B* **2006**, *110*, 10970–10981.

(20) Spanget-Larsen, J.; Gil, M.; Gorski, A.; Blake, D. M.; Waluk, J.; Radziszewski, J. G. *J. Am. Chem. Soc.* **2001**, *123*, 11253–11261.

(21) Mukherjee, A.; McGlashen, M. L.; Spiro, T. G. *J. Phys. Chem.* **1995**, *99*, 4912–4917.

(22) Tripathy, G. N. R.; Schuler, R. H. *J. Chem. Phys.* **1984**, *81*, 113–121.

(23) Berthomieu, C.; Boullais, C.; Neumann, J.-M.; Boussac, A. *Biochim. Biophys. Acta* **1998**, *1365*, 112–116.

(24) See, for example: Chipman, D. M.; Liu, R.; Zhou, X.; Pulay, P. *J. Chem. Phys.* **1994**, *100*, 5023–5036, and references therein.

(25) Hulsebosch, R. J.; van den Brink, J. S.; Nieuwenhuis, S. A. M.; Gast, P.; Raap, J.; Lugtenburg, J.; Hoff, A. J. *J. Am. Chem. Soc.* **1997**, *119*, 8685–8694.

(26) Barry, B. A.; El-Deeh, M. K.; Sandusky, P. O.; Babcock, G. T. *J. Biol. Chem.* **1990**, *265*, 20139–20143.

(27) Liu, R.; Zbou, X. *J. Phys. Chem.* **1993**, *97*, 9613–9617.

(28) Nwobi, O.; Higgins, J.; Zhou, X.; Liu, R. *Chem. Phys. Lett.* **1997**, *272*, 155–161.

(29) Qin, Y.; Wheeler, R. A. *J. Phys. Chem.* **1996**, *100*, 10554–10563.

(30) Schmidt, M. W.; Baldridge, K. K.; Boatz, J. A.; Elbert, S. T.; Gordon, M. S.; Jensen, J. H.; Koseki, S.; Matsunaga, K.; Nguyen, K. A.; Su, S.; Windus, T. L.; Dupuis, M.; Montgomery, J. A., Jr. *J. Comput. Chem.* **1993**, *14*, 1347–1363.

(31) Frisch, M. J.; Pople, J. A.; Binkley, J. S. J. *Chem. Phys.* **1984**, *80*, 3265–3269.

(32) Becke, A. D. *Phys. Rev.* **1988**, *A38*, 3098–3100.

(33) Slater, J. C. *Phys. Rev.* **1951**, *81*, 385–390.

(34) (a) Lee, C.; Yang, W.; Parr, R. G. *Phys. Rev.* **1988**, *B37*, 785–789. (b) Miehlich, B.; Savin, A.; Stoll, H.; Preuss, H. *Chem. Phys. Lett.* **1989**, *157*, 200–206.

(35) Vosko, S. H.; Wilk, L.; Nusair, M. *Can. J. Phys.* **1980**, *58*, 1200–1211.

(36) (a) Pulay, P.; Fogarasi, G.; Pang, F.; Boggs, J. E. *J. Am. Chem. Soc.* **1979**, *101*, 2550–2560. (b) Fogarasi, G.; Zhou, X.; Taylor, P. W.; Pulay, P. *J. Am. Chem. Soc.* **1992**, *114*, 8191–8201.

(37) Mayer, I. *Int. J. Quantum Chem.* **1986**, *29*, 477–483.

(38) Berthomieu, C.; Boussac, A. *Biospectroscopy* **1995**, *1*, 187–206.

(39) Takeuchi, H.; Watanabe, N.; Harada, I. *Spectrochim. Acta* **1988**, *44A*, 749–761.

(40) Grafton, A.; Wheeler, R. A. *J. Comput. Chem.* **1998**, *19*, 1663–1674.

(41) Xu, X.; Goddard, W. A., III. *Proc. Natl. Acad. Sci. U.S.A.* **2004**, *101*, 2673–2677.

(42) Santra, B.; Michaelides, A.; Schaffler, M. *J. Chem. Phys.* **2007**, *127*, 184104/1–184104/9.

(43) Adamo, C.; Barone, V. *J. Chem. Phys.* **1999**, *110*, 6158–6170.

(44) Hellwig, P.; Pfitzner, U.; Behr, J.; Rost, B.; Pesavento, R. P.; Donk, W. v.; Gennis, R. B.; Michel, H.; Ludwig, B.; Mäntele, W. *Biochemistry* **2002**, *41*, 9116–9125.

(45) Pulay, P.; Torok, F. *Acta Chim. Acad. Sci. Hung.* **1966**, *47*, 273–297.

(46) Boatz, J. A.; Gordon, M. S. *J. Phys. Chem.* **1989**, *93*, 1819–1826.

(47) Graphic generated using MacMolPlt v7.1. Bode, B. M.; Gordon, M. S. *J. Mol. Graphics Modell.* **1998**, *16*, 133–138.

(48) Grace, L. I.; Cohen, R.; Dunn, T. M.; Lubman, D. M.; de Vries, M. S. *J. Mol. Spectrosc.* **2002**, *215*, 204–219.

JP800169W